Defect and damage analysis of advanced discontinuous carbon/epoxy composite materials

Paolo Feraboli [a,*], Tyler Cleveland [b], Marco Ciccu [b], Patrick Stickler [c], Luciano DeOto [d]

[a] Automobili Lamborghini Advanced Composite Structures Laboratory, Department of Aeronautics and Astronautics, Box 352400, Guggenheim Hall, University of Washington, Seattle, WA 98195-2400, United States
[b] Department of Aeronautics and Astronautics, University of Washington, Seattle, WA, United States
[c] Boeing 787 Technology Integration, Boeing Commercial Airplanes, The Boeing Co., Everett, WA, United States
[d] Advanced Composites Development Center, Automobili Lamborghini S.p.A., Sant'Agata Bolognese, Italy 40019, Italy

ARTICLE INFO

ABSTRACT

Recent composite technology research and development efforts have focused on discontinuous carbon fiber/epoxy molding systems derived from chopped aerospace-grade unidirectional tape prepreg. This study analyzes in detail the meso-structure of this class of materials, which exhibit point-to-point variations associated with the random chip distribution, by means of destructive and non-destructive inspections, in the attempt to identify characteristic traits that can yield insight in its quality and performance. Results show that several types of defects can be encountered within the molded panel, such as macro-voids, fiber kinking and swirling, or resin-rich areas. However, it is found that failure may or may not occur in proximity of these hot spots, independently from their size and location, even for specimens containing the circular hole. Therefore it appears that for this class of materials conventional ultrasonic inspection and defect classification may not be suitable as criteria for part acceptance or rejection.

1. Introduction

Recent composite technology research and development efforts have focused on new out-of-autoclave material forms, and automated processes that can markedly increase production efficiencies. The interest of the aerospace community for short fiber composites, such as Sheet Molding Compounds (SMC), dates back to the 1960s and the pioneering work of Halpin, Pagano and Kardos [1–3]. In recent years, airframe manufacturers have been proposing the use of high-performance discontinuous systems that are suitable for compression molding of primary structures. Commercial applications for this type of material form already exist, although using different resin systems and fiber types and lengths, under various manufacturers and trade names (e.g. Quantum Lytex 4149 and Hexcel HexMC®). The Boeing 787 Dreamliner for example makes use of AS4/8552 HexMC® for the window frames [4,5], as well as other primary and secondary structural elements. These mats are processed by consolidating sheets of randomly-distributed "chips", up to 2.0 in. long and 0.33 in. wide (50.8 mm × 8.4 mm) in the form of a roll. These chips are obtained from pristine aerospace-grade unidirectional (UD) carbon fiber/epoxy prepreg, which is first slit longitudinally and then chopped. Although the raw material cost associated with these chopped systems is higher than the UD prepreg from which they are derived, their suitability to be molded in complex geometries with lower manufacturing costs and at higher rates can justify their adoption to reduce overall part acquisition costs.

The authors have been performing fundamental research on these materials, and previous experimental results have been reported [6–8]. This class of materials, which sits between traditional SMC and prepreg tape, has shown excellent mechanical properties [5,6], particularly for stiffness-dominated designs, since the average modulus reported can be as high as that of the reference quasi-isotropic continuous tape laminate. Furthermore, while tensile strength is less than half that of the reference quasi-isotropic continuous tape laminate, compressive and shear strengths are much closer to those of the reference tape laminate. If material and process are accurately controlled, the variation observed in the measured strength is also relatively low around 8%, and competitive with the 4–6% observed for the tape precursor. Results also show that the distribution of chips is indeed random, yielding in-plane quasi-isotropic elastic and strength properties. These statements have been verified by testing coupons obtained at 0°, 45° and 90° directions.

These materials also pose unique challenges for engineers tasked with design, analysis and certification of primary structural parts manufactured with them. In particular, two unique characteristics have been reported in [7,8] respectively. The open-hole tension strength of these materials has been shown [7] to be

---

* Corresponding author.
  E-mail address: feraboli@aa.washington.edu (P. Feraboli).

virtually notch-insensitive at the macroscopic level, possibly due to the presence of internal stress concentrations arising from the heterogeneous nature of the sub-structure. This sub-structure can be identified as a meso-structure rather than a micro-structure, since it appears to be associated to the size and properties of the chips, rather than to the characteristics of the constitutive fiber and resin phases. An "inherent material" stress concentration factor is derived, and used to explain the tendency of the material to often fail at the gross-section regardless of the presence of a hole. This behavior is hole size-dependent and it transitions to exclusive net-section failure for large hole sizes. Common analysis methods used for homogenous materials, independent from their orthotropic nature, cannot be used to predict notched strength load and location of failure, although it was shown that a modified Point Stress Criterion employing large characteristic length values could be used. The non-homogeneous meso-structure appears to be responsible also for the observations in [8], where axial Young's modulus measurements, conventionally obtained by strain gage or extensometer, yield up to 19% Coefficient of Variation (CoV) from specimen to specimen as well as within a single specimen. A series of tensile tests was conducted while systematically varying strain gage length, from 0.125 in. up to 2.0 in. (3.2–50.8 mm), as well as strain gage and extensometer location along the length and across the width of the specimen. Values have been measured in different locations on the same specimen that vary from as low as 3.0 Msi to as high as 9.0 Msi (20.68–62.04 GPa). Longer strain gages do not appear to yield better results than shorter gages, and extensometer readings are not necessarily better than strain gage ones, thus suggesting that the length scale associated with these strain/modulus variations is greater than what can be measured with a large strain gage. The use of Digital Image Correlation technique (DIC) to obtain full-field strain distributions on the surface of the specimen revealed a complex state of variable strain in the specimen, with peaks and valleys throughout the specimen. It also allowed for obtaining the most comprehensive modulus measurement by averaging the strain values over the entire surface of the tensile coupon, and thus showing that the average material modulus is indeed relatively constant with 5% CoV. These observations support that the observed variation in local modulus are peculiar to this material, whose heterogeneous meso-structure is comprised of highly orthotropic and long reinforcements.

2. Material fabrication and test setup

All discontinuous carbon/epoxy specimens are manufactured in the laboratory starting from unidirectional tape prepreg. The system is a 350 °F cure (177 °C), designated for vacuum bag, autoclave cure, and has a resin content of 45%. During molding, 2–3% by volume or resin is lost in flash and through vent holes, which are used to evacuate air, so that the final fiber volume content is around 57–78%. The chip dimensions are 2.0 in. long × 0.33 in. wide (50.8 mm × 8.4 mm). Detailed discussion of the compression molding manufacturing process for the material is reported in [6]. After extraction from the mold, the panel is trimmed 1.0 in. (25.4 mm) on all sides to remove the regions of high flow toward the mold edges, where it is more likely that chip alignment and distortion may occur, Fig. 1. Although this is a low-flow process, unlike typical SMC molding where the charge covers only a small fraction of the mold, some degree of resin flow still takes place during the molding process. This is not sufficient to create a noticeable alignment of the fibers along any preferred direction, but inevitably lead to the formation of small resin-rich areas. Average panel thickness is 0.165 in. (4.2 mm), and corresponds to a nominal number of 32 chips through the thickness, each with a cured thickness of 0.005 in. (0.13 mm), Fig. 2.
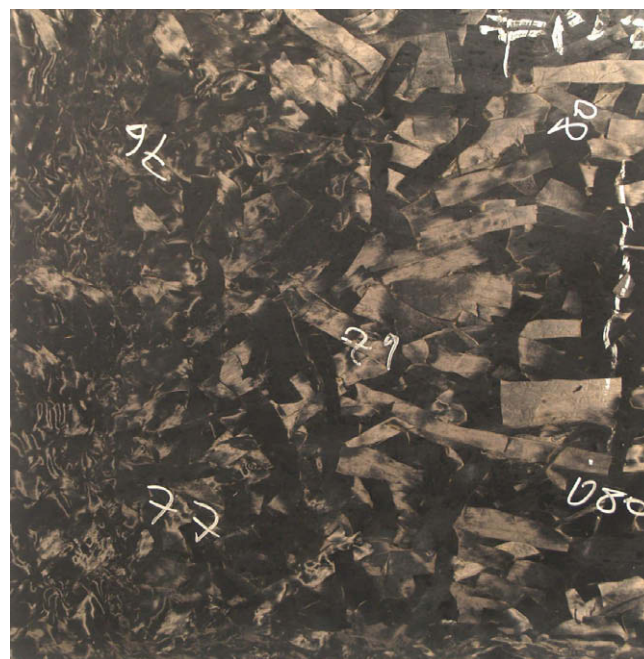
Fig. 1. Molded and trimmed panel.

A total of 24 specimens are evaluated, as summarized in Table 1, and include a broad range of physical and mechanical property evaluations. Non-destructive evaluation (NDE) is performed by means of pulse-echo C-scan ultrasound, a Physical Acoustics Corp. UltraPAC NDT Automation immersion system, using a 5 MHz sensor. The multichromatic scale ranges from red, which indicates no signal loss, to blue,[1] or complete loss of signal, Fig. 3. The signal threshold is set at 6 dB loss, which corresponds to 80% of the emitted signal. As it can be seen, the bulk of the laminate is comprised of a diffused mix or red, orange and yellow areas, which indicate a highly heterogeneous structure. C-scan images are difficult to interpret compared to tape laminates. With ultrasonic inspection, any change in material properties, such as the presence of a defect or of a thickness transition, is characterized by attenuation in the signal. For this material form, there are point-to-point variations in material properties due to the random chip distribution, which generates signal attenuation often not corresponding to the presence of a true defect. It becomes difficult to isolate the presence of a small defect from the background noise. However, a few small regions are indicated with green and blue, and are indicative of regions where the signal attenuation is greater than the surrounding material. These regions are here defined as "hot spots", or regions of interest, as it is not possible to define them as true defects without further characterization.

Pulsed thermography is used to evaluate its suitability to better detect the presence of damage. Thermal Wave Imaging, Inc. is subcontracted to perform non-destructive inspection of a selected number of panels using their Echotherm Infrared Flash Thermography system. The image of Fig. 4 shows that for this material system thermography is not a suitable tool to detect the presence of small manufacturing defects, or hot-spots. Using the 5 MHz frequency as the benchmark for ultrasonic inspection, sensor frequencies of 2.25 and 10 MHz are evaluated to assess their ability to isolate the presence of hot spots from the-background noise, Fig. 5. It can be seen that at 10 MHz the image shows a greater number of regions of signal attenuation, but the increased sensitivity and detail is hindered

---

[1] For interpretation of color in Figs. 3, 8 and 10, the reader is referred to the web version of this article.
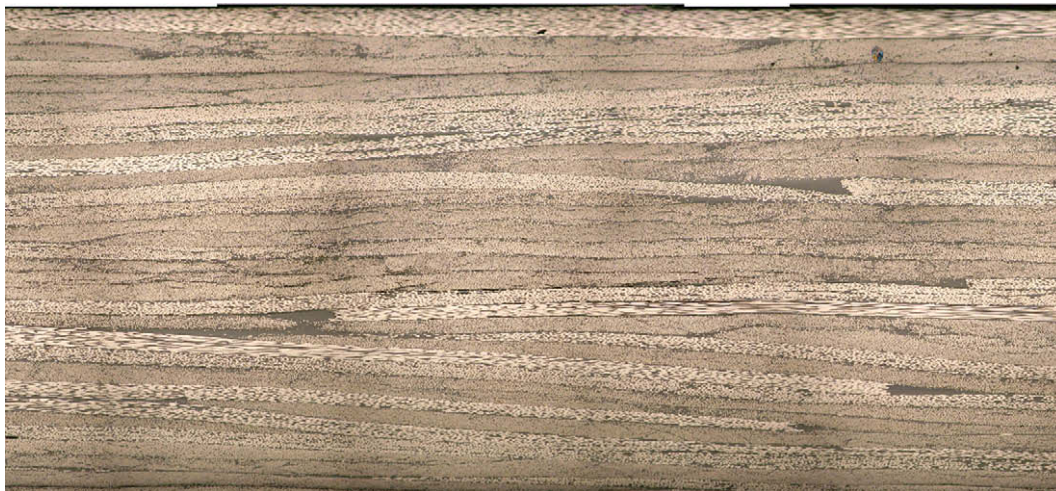
Fig. 2. Typical cross section of pristine (high quality) material, showing the randomly oriented chips alternating through the thickness.

Table 1
Summary of specimens evaluated in this study.

Specimen #	NDE	Final operation	Ultimate strength [ksi] (MPa)
1	C-scan/thermography	Two hot-spot regions microscopy	–
2	C-scan	Three hot-spot regions microscopy	–
3	C-scan/thermography	Two hot-spot regions microscopy	–
4	C-scan	Four hot-spot regions microscopy	–
5	C-scan	Three regions of acid digestion	–
6	C-scan	Three regions of acid digestion	–
7	C-scan	Surface machining	–
8	C-scan	Surface machining	–
9	C-scan before and after failure	Load to ultimate failure	45.4 (313)
10	C-scan before and after failure	Load to ultimate failure	41.3 (285)
11	C-scan before and after failure	Load to ultimate failure	46.4 (320)
12	C-scan before and after failure	Load to ultimate failure	49.5 (341)
13	Progressive C-scan up to failure	Progressive loading up to failure	44.4 (306)
14	Progressive C-scan up to failure	Progressive loading up to failure	54.1 (373)
15	Progressive C-scan up to failure	Progressive loading up to failure	41.2 (284)
16	C-scan before and after loading to 70% of ultimate	Hot-spot growth microscopy	–
17	C-scan before and after loading to 80% of ultimate	Hot-spot growth microscopy	–
18	C-scan before and after failure	Load to ultimate failure in presence of open hole	46.6 (321)
19	C-scan before and after failure	Load to ultimate failure in presence of open hole	41.1 (283)
20	C-scan before and after failure	Load to ultimate failure in presence of open hole	44.3 (305)
21	C-scan before and after failure	Load to ultimate failure in presence of open hole	43.6 (301)
22	Progressive C-scan up to failure	Progressive loading up to failure in presence of open hole	39.5 (272)
23	Progressive C-scan up to failure	Progressive loading up to failure in presence of open hole	45.9 (316)
24	Progressive C-scan up to failure	Progressive loading up to failure in presence of open hole	36.3 (250)

by a greater difficulty to discriminate these regions from the background noise. On the other hand, the 2.25 MHz sensor shows a much smoother signal contour, and the areas of signal attenuation are clearly defined. However, the image loses sufficient detail to change the shape and size of some key regions of signal attenuation, and in some cases completely misses them. For these reasons, ultrasonic inspection using the 5 MHz sensor is deemed the most suitable NDE technique, giving the best compromise between sensitivity and noise, and will be used for the rest of this study.

Micrographic coupons are extracted from molded panels in the regions where the ultrasound indicates the presence of a hot spot. Since the panels have random chip distribution and have been shown to be quasi-isotropic in the plane, the orientation of the cross section cut is not relevant. The specimen is first vacuum-impregnated with mounting epoxy resin, then pressure-cured to minimize formation of air bubbles, and is finally polished for inspection. The specimen is polished with a 6-step process: 180 grit, 600 grit, 1200 grit, 9-µm, 3-µm silk, 3-µm non-nap poly-

ester and ending up with 1 h polishing with a non-nap polyester cloth and 10% alumina solution. Magnification from $50\times$ to $500\times$ is used to detect the nature of the hot spots, and to observe the presence of damage.

A selected number of specimens are machined from the molded panel to smaller size, approximately 1.5 in. × 3.0 in. (38.10 mm × 76.20 mm). Following ultrasonic inspection to detect the presence of hot spots, these are mounted on a milling machine and subjected to further machining. From the top surface, the surface is milled at 0.0025 in. (0.06 mm) increments through the thickness, corresponding to half the chip thickness. Since the ultrasonic image shows only a projected hot spot area, it is not easy to determine its depth within the laminate. By removing "planes" of material at each step it is possible to expose the underlying micro-structure and observe by optical microscopy the nature and location of the hot spots.

Six small specimens, having a weight of 1 g, are evaluated for fiber volume content by means of ASTM standard D3171 for acid
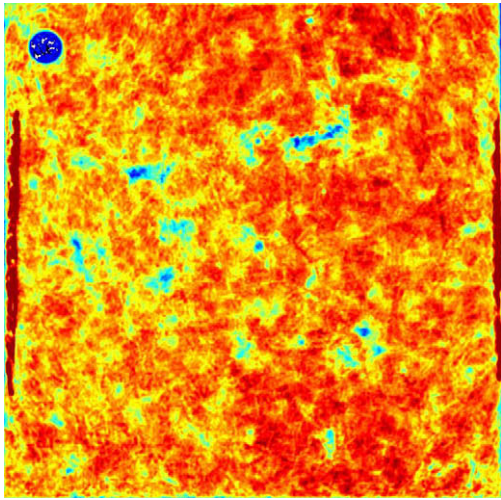
Fig. 3. C-scan pulse-echo ultrasonic image of a molded panel using a 5 MHz sensor.
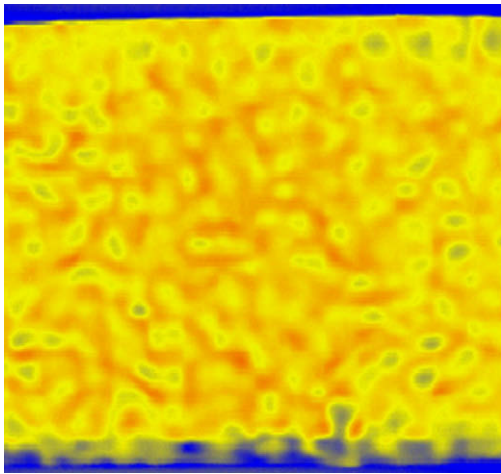
Fig. 4. Pulsed thermography analysis of molded panel in Fig. 3, courtesy of Thermal Wave Imaging Inc.
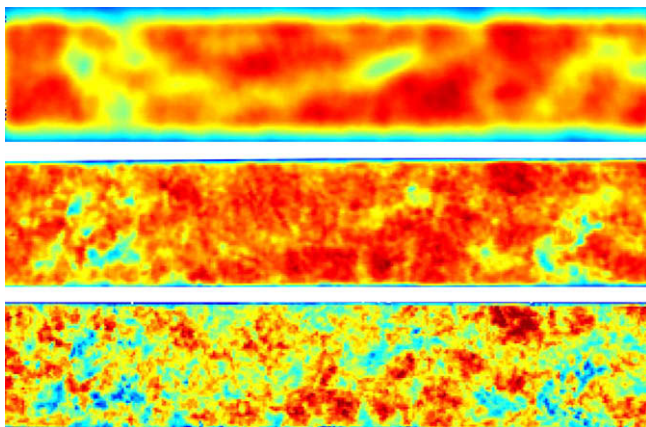
Fig. 5. C-scan pulse-echo ultrasonic image of a specimen using 2.25, 5 and 10 MHz sensors (top to bottom).

digestion [9]. After measuring the volume of the composite specimen by immersion in distilled water, the specimens are immersed in a beaker containing a 20 ml of sulphuric acid and heated on a hot plate to boiling temperature. At that point 35 ml of hydrogen peroxide are added to clarify the mixture, which indicates that indicates that the resin is fully dissolved. While the epoxy matrix dissolves in acid, the fibers are unaffected by the corrosive mixture. The residue is cooled down in cold water and filtered in 15-μm ceramic filters using a vacuum pump to separate the liquid, which is the collected in a catcher. After desiccation, the left over fibers are weighed to measure the remaining volume. The difference between the composite specimen volume before acid digestion and the volume of the left over fibers gives a measure of the resin volume content. It should be emphasized that this process is very slow and lengthy, and selection of the appropriate filters as a compromise between process time and measurement accuracy is key. The burn-off test, which can be used to separate resin from fibers by ignition loss in a furnace, is a much speedier process and less operator intensive. Although preferable from a user perspective, such test can be used only for glass fibers, since carbon fibers carbonize and vaporize at high temperatures.

From the molded panels, tensile specimens are machined to the Boeing standard test method for unnotched tension [10]. The specimens have straight-sided rectangular geometry with dimensions 12.0 in. × 1.5 in. (304.80 mm × 38.10 mm). Since glass/epoxy fabric tabs of length 2.0 in. (25.4 mm) are bonded to the specimen using 3 M Scotchweld film adhesive, the effective gage length is reduced to 8.0 in. (203.2 mm). All specimens are loaded at a rate of 0.05 in./min (1.3 mm/min) in a 2-grip Instron hydraulic tension/compression test frame. From previous research [6–8], the authors had identified the average tensile failure strength of this material. In this study, the specimens are loaded progressively to failure at increments of 60%, 70%, 80%, 90% and 100% of the average ultimate failure strength. After each loading step, the specimens are removed and inspected via ultrasound to monitor the initiation of damage and the growth of hot spots. After inspection, the specimens are re-positioned in the test frame and the loading is increased to the next step. For a selected number of specimens, the load is interrupted at one of the step and the specimen is sacrificed for destructive inspection. Microscopy is used to evaluate the nature of the damage and its extent.

3. Defect inspection and characterization

Ultrasonic C-scan inspection is used on specimens #1–4 to detect the presence and location of hot spots, but only two specimens are shown in this section, as they are sufficiently representative of the whole set. At the location of the hot spots, the specimens are sectioned to obtain smaller specimens for micrographic inspection. Specimen #2 is shown in Fig. 6, and highlights the presence of three well-defined regions of signal attenuation, indicated in blue. The micrographic images associated with each of the hot spots are shown on the right. At position 1, the hot spot is associated with the presence of a large swirl, which is a region of extensive chip kinking and distortion associated to a region of high flow. As mentioned previously, although these materials are designed to be low-flow, that is the majority of the mold cavity is covered by the charge, in some regions higher flow may occur due to an inconsistency in the charge distribution. Positions 2 and 3, in the same specimen, show large resin pockets, one toward the surface and the other toward the midplane of the laminate. During molding the resin liquefies and fills the interstices left between neighboring chips. While this is a desired attribute, if the mat used in the charge exhibits a particularly large empty space, for example associated with a missing chip, the resin will concentrate in this region and form resin-rich pockets. Specimen #4, Fig. 7, exhibits two hot spots, which both reveal to be associated to the presence of several large voids. These macro-voids are much larger than the typical
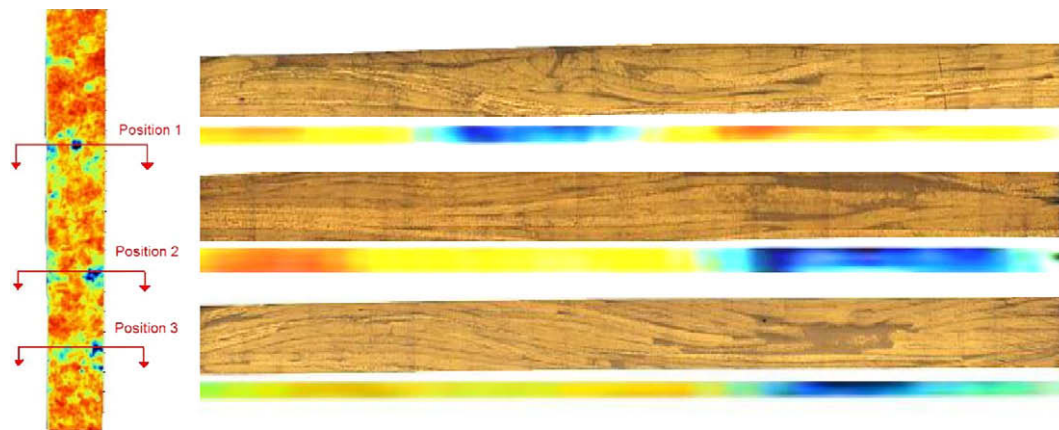
Fig. 6. Micrographic images of three different hot-spot regions in the specimen #2 shown on the left.
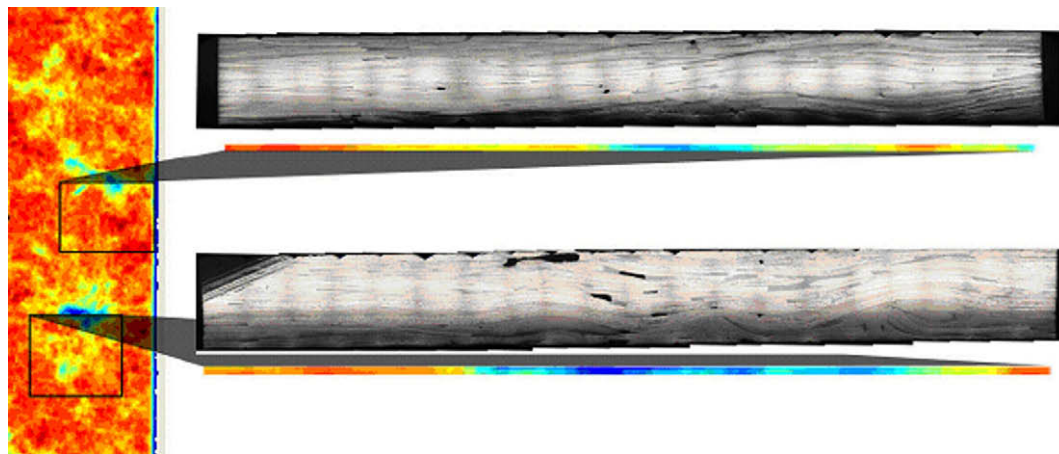
Fig. 7. Micrographic images of two different hot-spot regions in the specimen #4 shown on the left.

voids associated with the diffused porosity encountered in autoclave processing, and form during manufacturing when air bubbles are entrapped in the laminate. Because of the high pressures involved in manufacturing these materials, ranging from 750 to 1200 psi (51.7 and 82.8 bars respectively), porosity is not a typical problem. Typical prepreg autoclave cure is performed at much lower pressures, ranging from 80 to 100 psi, or 5.5 and 6.9 bars respectively. On the other hand, because the pressures are so high and the curing time so low (approximately 5–20 min in the press, compared to the several hours used for autoclave curing), any air bubble entrapped in the charge will not have a chance to escape. It should be noted that one of the two hot spots of specimen #4, the one on the lower left in Fig. 7, corresponds to a small mark on the outer surface of the panel. Such defects, that are detectable by visual inspection, have the advantage that can be accounted for during quality acceptance screening.

Specimens #5 and #6 are used for acid digestion testing. For each panel, three specimens are identified by C-scan as corresponding to a region of pristine signal (red/orange), of partial signal attenuation (green/light blue), and of high signal attenuation (dark blue), Fig. 8. Results show that the pristine regions have high fiber volume content of 59%, regions of modest attenuation have an average of 55.5%, while regions of high attenuation have an average of 53.7%. These results confirm the microscopic analysis observations, which seem to indicate that these hot spots are associated to macro-voids, chip swirls or resin-rich areas, all of which are characterized by low fiber volume content.

Specimens #7 and #8 are first inspected by C-scan to reveal the presence of hot spots, whose nature location through the thickness is not discernible based on the ultrasonic image alone. They are then placed in a milling machine and subjected to material removal from the top surface down. This process can be performed across the entire surface of the specimen at the same time, or at subsequent steps, Fig. 9A. By superimposing the C-scan image to the machined surface it is possible to focus on the locations of the hot spots, Fig. 9B. After each pass, which is associated with the removal of half a chip thickness, the specimen is inspected under the microscope to verify if the hot spot is visible. From the surface of the specimen in Fig. 9C it is possible to see the presence of macro-voids, visible as either small concave regions or striations, which indicate an elongated shape. The material removal operation is very time-consuming, and does not yield particular insight on the nature of the defects, although it does supply an interesting view of the meso-structure of the material along planes parallel to outer surfaces. Since the chips do not remain perfectly aligned during the molding process, this structure is characterized by highly heterogeneous collection of pseudo-elliptical regions having different chip orientations, Fig. 9D.

4. Damage growth and failure

Specimens #9–12 are selected based on ultrasonic inspection that contain several hot-spot regions, with the intent to see how these may affect failure load and location. The hot spots vary in
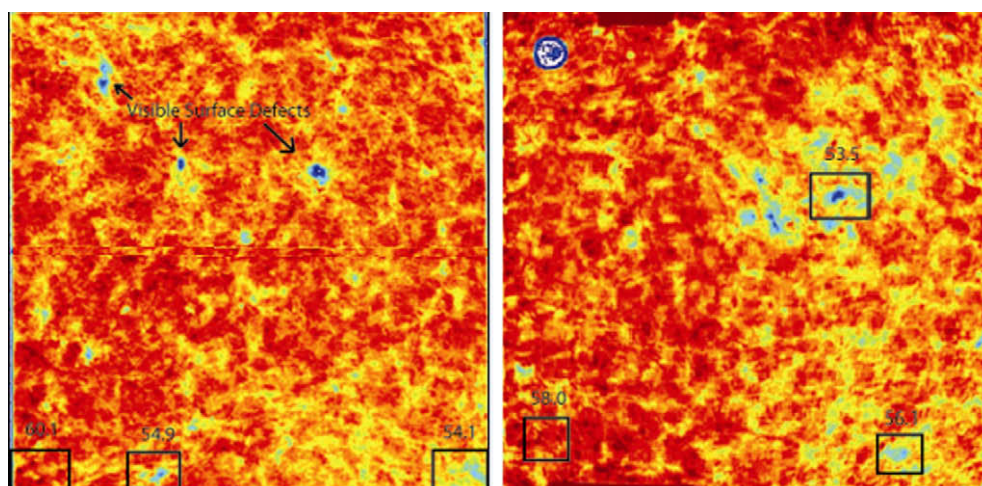
Fig. 8. Acid digestion locations and fiber volume content results for specimens #5 and #6.

size, location and intensity, as seen in Fig. 10, and include some that are of high intensity (dark blue) but relatively isolated, and others that are less intense (light blue) but more diffused throughout the specimens. The larger hot spots are then traced out on the surface of the specimens by means of a white marker to monitor if failure occurs at these locations, Fig. 11. The specimens are then loaded to ultimate failure and inspected by ultrasound again, Fig. 10. Three of the four specimens failed in the gage section, while one (specimen 15) failed in proximity of the tabs. Although specimen #9 contains two large hot spots toward the upper and lower parts of the image, failure occurs at a milder hot spot, located toward the center gage of the specimen. Specimen #10 contains 8 mild hot-spot regions dispersed along the specimen, of which one appears to be slightly more intense than others. Failure occurs in the center section in an area that is characterized by relatively mild and spaced hot spots, while the larger hot spot seems unaffected in size and intensity. On the other hand, two of the milder hot spots, one toward the upper part of the specimen, and one toward the lower part, have grown significantly in size and intensity during loading. Specimen #11 fails at the tabs, in proximity of the grips, but a closer look reveals that a relatively dense number of hot spots exist in that region prior to loading. From the post-failure ultrasound, it appears that these hot spots grow and coalesce during loading, leading to failure in that region close to the tabs. Another large hot spot region has grown during loading toward the bottom of the specimen, in a region that was apparently free of hot spots, and at failure its size and intensity is nearly as large as that where failure occurred. Specimen #12 contains 7 hot-spot regions, the majority of which are concentrated on the left side of the specimen in Figs. 10 and 11. The largest one, in the shape of a T, is located toward the center section of the specimen, and is in close proximity to another large hot spot. Failure occurs in that region after those two hot spots grow and coalesce. It should be noted that toward the bottom of the specimen, two other hot spots, located on the opposite sides of the centerline, have grown significantly and started to coalesce.

Preliminary observations coming from these tests are that ultimate failure may manifest in proximity of the dominant hot spot, but in at least 50% of the cases it may occur either in a region of neighboring hot spots of lower intensity or even in a region of apparently pristine ultrasonic area. Unlike continuous fiber composites, the intensity and size of the defect, or hot spot as it is here called, may not dictate the location of failure. Secondly, during loading some of these hot spots grow in size, and neighboring ones tend to coalesce. However, not all hot spots show the same growth

behavior, and some of the larger, more intense ones may not grow at all.

In order to better capture the evolution of damage and the growth of these hot spots, three tensile specimens are loaded at increments up to catastrophic failure. After each loading increment, the specimen is removed from the test frame and inspected via C-scan. By means of image analysis, the total "damage area" is measured, which is defined as the area of the specimen exceeding a predefined threshold for signal attenuation. Progressive C-scan images are shown for specimens #13–15 in Figs. 12–14. Each figure shows six C-scan images, corresponding to six fractions of ultimate load: 0% (pristine specimen), 60%, 70%, 80%, 90%, and 100% (ultimate load and failure). Specimen #13, Fig. 12, shows the presence of a large, intense hot spot prior to loading. Such hot spot does not grow significantly during loading, and ultimately does not precipitate failure in its proximity. Failure occurs on the right side of the specimen, in an apparently pristine region, where few mild hot-spot regions grow during loading and coalesce. Specimen #14, Fig. 13, shows the presence of several hot spot region of high signal attenuation, with the largest one toward the right of the specimen and in proximity of other two slightly smaller regions. During loading all hot spots grow in size and intensity, and finally failure precipitates when the two hot spots on the right coalesce. For specimen #15, Fig. 14, only four C-scan images are shown since it fails prematurely at 90% of the average ultimate strength of the material. The specimen exhibits a small but intense hot spot in its right side, and two areas of diffused but low-intensity signal attenuation, in the center and to the left of the specimen. Upon loading, the left-most region grows at a much faster rate than the other hot-spot regions, including the high intensity one on the right, and eventually leads to failure. For all specimens the growth is sudden, and at 60% and 70% of ultimate load the change in damage area is virtually undetectable. For the three specimens tested, Fig. 15 shows that at 60% of ultimate load there is virtually no change in the total area of signal attenuation, while at 70% the area is between 10% and 20% larger than the pristine value. Only at 80% of ultimate load the growth becomes evident, at approximately 50% more than the pristine value, and increases more rapidly at higher load values, reaching 150% at 90% of loading.

Specimens #16 and #17 are inspected by ultrasound prior to being loaded to 70% and 80% of ultimate load respectively. They are then inspected by ultrasound again to verify the growth of the hot spots and initiation of damage, and are then sectioned for microscopic analysis to understand the damage mechanisms. Fig. 16 shows this process for specimen #16, from which three dif-
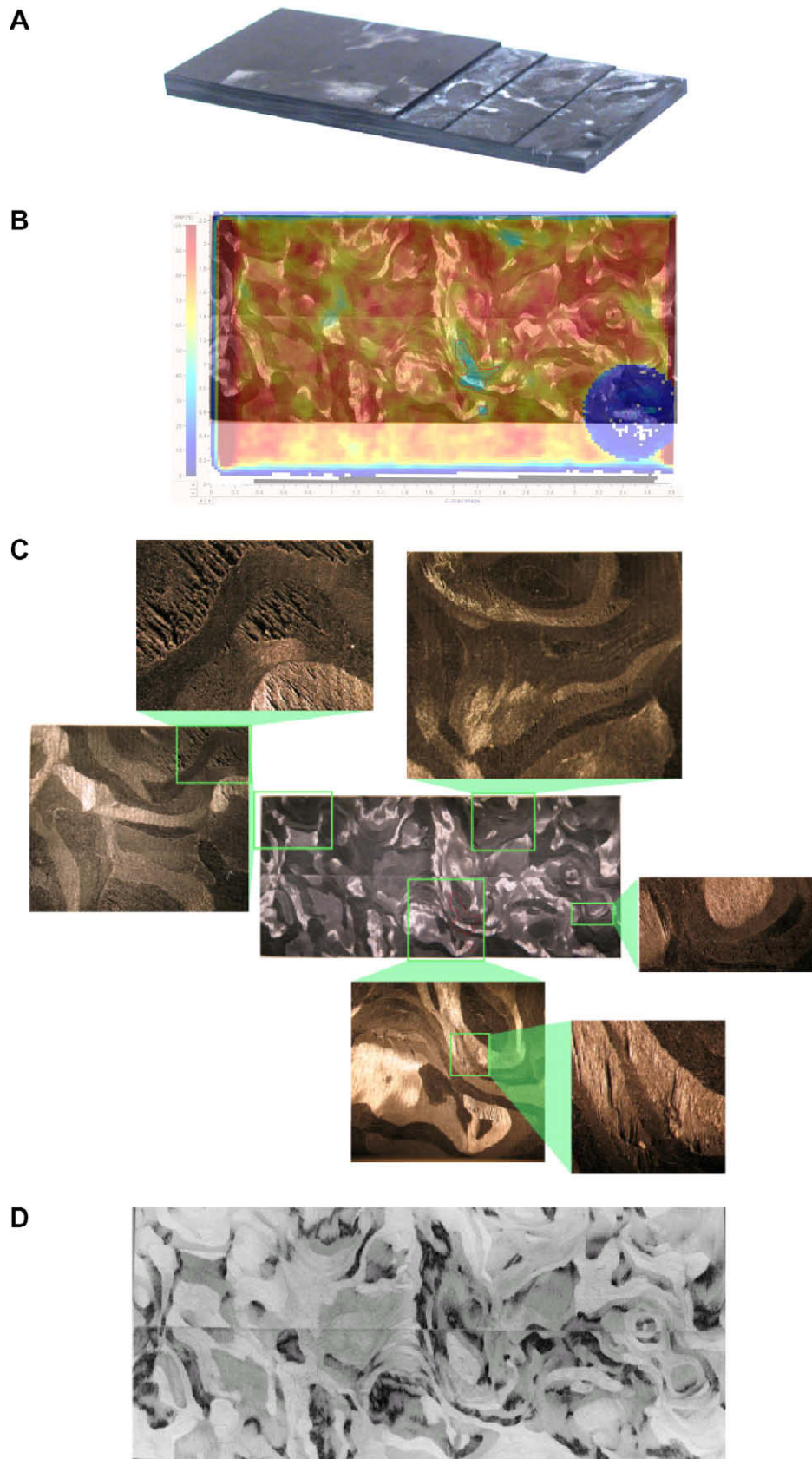
Fig. 9. (A–D) Top view of specimen #7 following surface machining to expose underlying structure and hot spots.

ferent regions are sectioned. These regions, which are designated M1–M3 and showed top to bottom in Fig. 16, include a region of apparent pristine conditions and no signal attenuation (M3), a region of intense signal attenuation (M2), and an intermediate attenuation region (M1). Section M2 shows a range of multiple defects that appear to concentrate in the same region. These include sev-
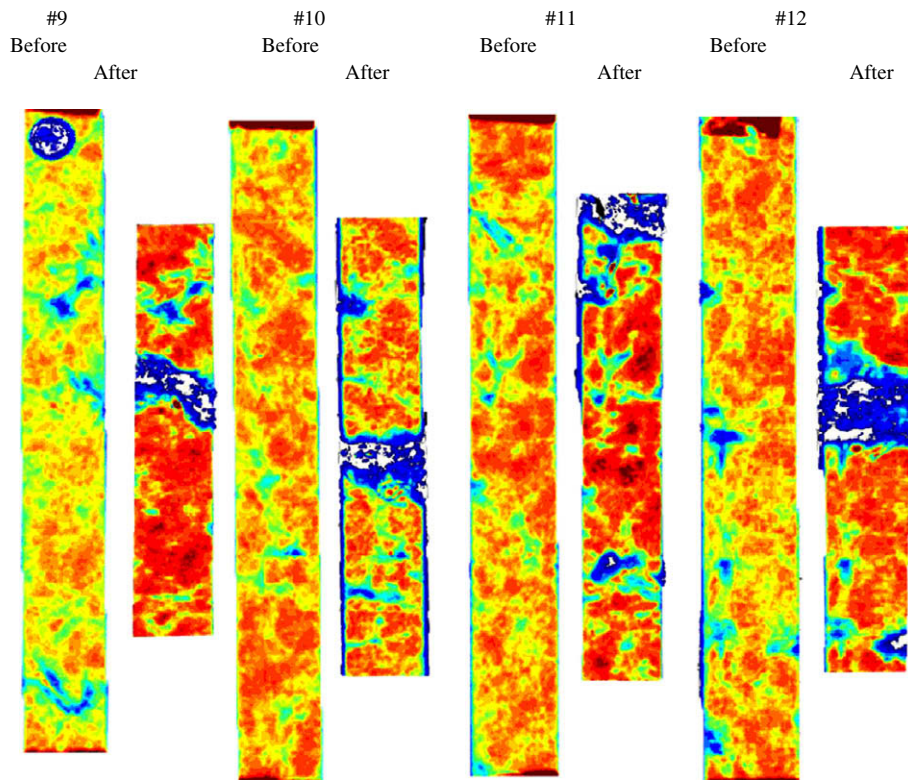
Fig. 10. Ultrasonic images of specimens #9–12 before and after failure.
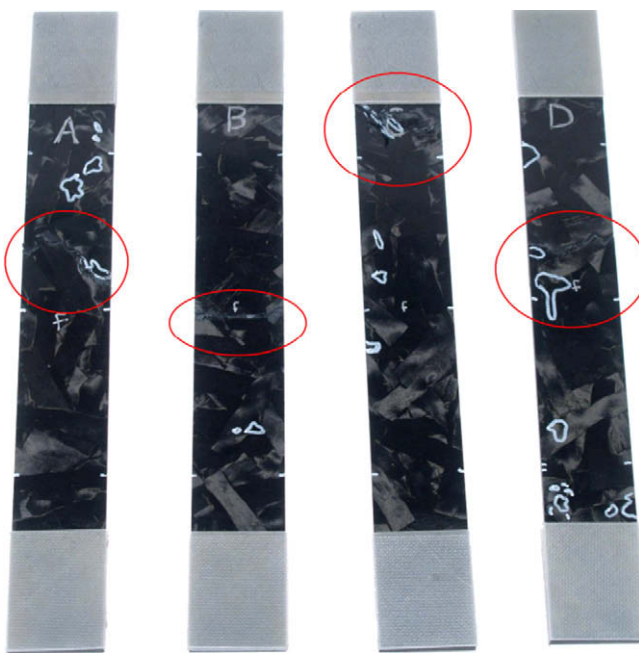
Fig. 11. Specimens #9–12 after failure.

eral macro-voids of varying sizes concentrated on the left side of the cross section, and a large swirl, or region of high flow and fiber kinking in the center of the cross section, Fig. 17. These are present before loading and do not show signs of growth. On the right side of the specimen, Fig. 18, several inter- and intra-chip cracks can be observed through the thickness, as well as multiple large adjacent delaminations, which appear to generate in resin-rich regions in the proximity of chip terminations. Both transverse cracks and del-

aminations are the result of the applied load and are responsible for the increase in total "damage" area, or area of signal attenuation as measured by C-scan. Section M1, Fig. 19, of mild signal attenuation exhibits the presence of several intra-chip cracks directed perpendicular to the cross section. These cracks are typical of the early stages of damage initiation and growth, and form in a region without obvious manufacturing flaws or apparent hot spots. Section M3, Fig. 20, which belongs to a bright red region of no signal attenuation, shows a pristine micro-structure as the one reported in Fig. 2. Similar observations from specimen #17 suggest that the relationship between large manufacturing defects, such as voids and swirls, and damage initiation and propagation appears to be all but obvious. Damage does not emanate and grow from the pre-existing defects, although it forms in their proximity. It is possible that the presence of defects may be responsible for locally lower mechanical properties, such as Young's modulus whose point-to-point variation is documented in [8], and in turn may create high strain gradients in their proximity. These gradients could then affect the local load redistribution and precipitate failure in the pristine material in proximity of these defects. In any case, the presence of hot spots, which are confirmed to be manufacturing defects of varying nature, does not consistently precipitate failure in their proximity.

It was previously reported by the authors in [7] that this material form is particularly notch-insensitive, and exhibits an open-hole tensile strength that is unchanged with respect to the unnotched strength. Furthermore, for 0.25-in. (6.35 mm) circular hole, it was reported that at least 50% of the specimens fail away from the open hole, in the gross section. It is thought that such behavior is due to the presence of defects, or hot spots, that create material stress concentrations more dominant than the geometric one. To validate this theory, a series of notched tensile tests are performed on specimens #18–21. Four specimens are selected carefully to ensure that no significant hot spots are present, as shown in the C-scan images of Fig. 20, which are characterized by a uniform red
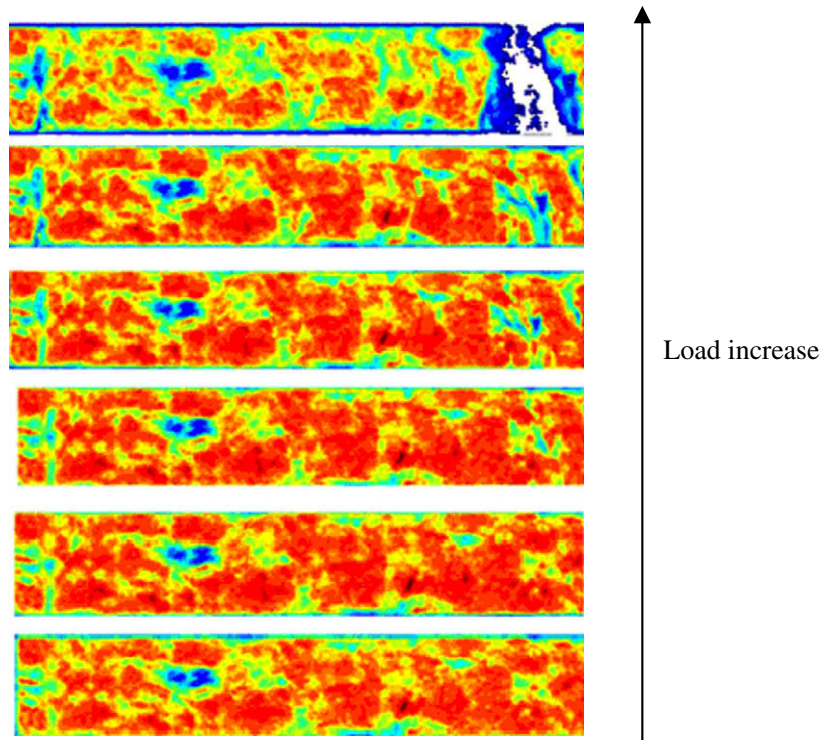
Fig. 12. Specimen #13 undergoing progressive loading and ultrasonic imaging up to ultimate failure.
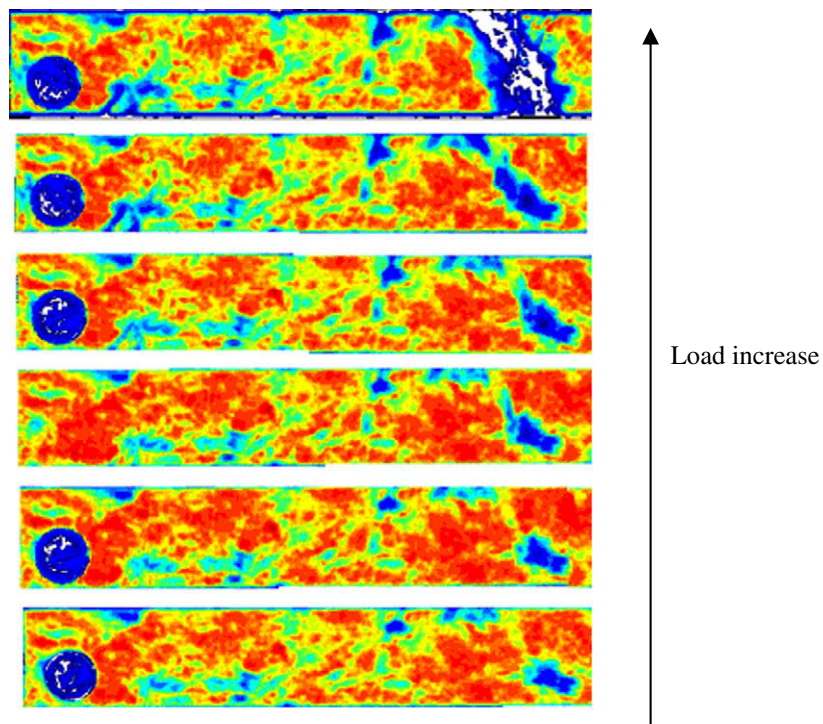
Fig. 13. Specimen #14 undergoing progressive loading and ultrasonic imaging up to ultimate failure.

(high signal) projected area. The specimens are then loaded to failure, but three of the four specimens fail away from the hole, in the gross section area. From the ultrasonic images it is not clear why failure precipitates at a specific point along the specimen, since there are no obvious regions of signal attenuation.

Another set of notched specimens is tested but, unlike the previous ones, these are selected to one or more hot spots, to understand if the presence of a clearly defined hot spot can precipitate failure in its proximity. Specimens #22–24 are loaded to failure at multiple increments, and between each loading step they are re-
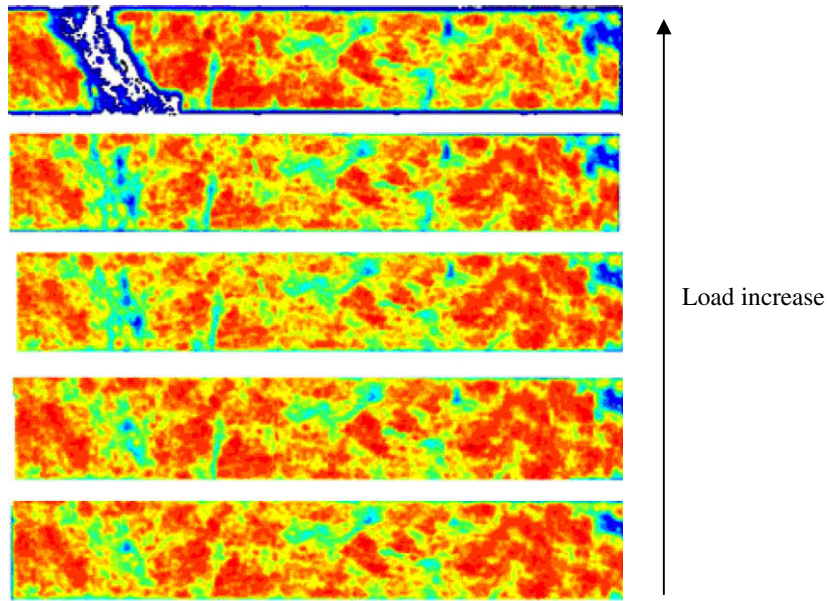
Fig. 14. Specimen #15 undergoing progressive loading and ultrasonic imaging up to ultimate failure.
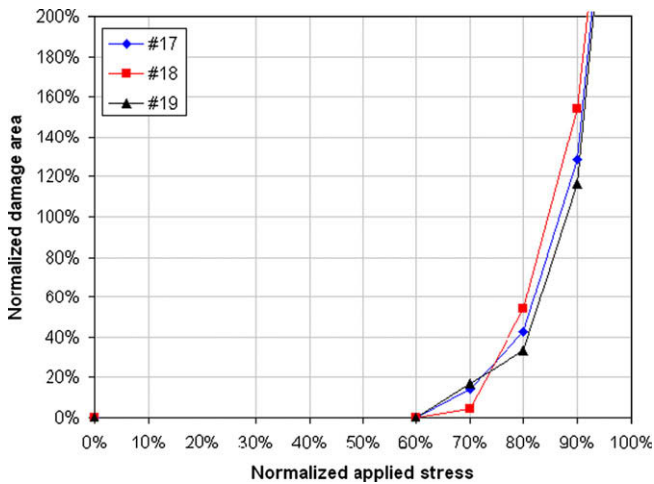
Fig. 15. Normalized damage area vs. normalized applied stress for the three specimens of Figs. 12–14.

moved and inspected via ultrasound to monitor the growth of damage. As in previous tests for unnotched specimens, five C-scan images are shown for each specimen, corresponding to 0% (unloaded), 50%, 70% 90% and 100% (ultimate failure) increments. Specimen #22, Fig. 21, contains a relatively large hot spot in the proximity of the open-hole. Upon loading, the hot spot grows across the specimen width in a direction away from the hole, and eventually leads to failure in the gross section, although close to the hole. During loading, two large hot spots form on the left side of the specimen, and at failure they have grown to the point that they almost coalesce. Specimen #23, Fig. 22, contains a mildly homogeneous signal, with no clearly defined hot spot. Upon loading, four/five mild hot spots begin to form at different locations along the specimen, and eventually two of them on opposite sides of the specimen width coalesce and precipitate failure. Specimen #24, Fig. 23, exhibits a high-intensity hot spot and a wide region of diffused mild-intensity hot spots to the left of the specimen. During loading these hot spots grow, and in particular the smaller but more intense one coalesces with a neighboring one and leads to failure.

Fig. 16. Specimen #16, inspected by ultrasound before and after loading to 70% of ultimate strength, is then sectioned in three different locations M1–M3.

Fig. 17. Detail of section M2, center.
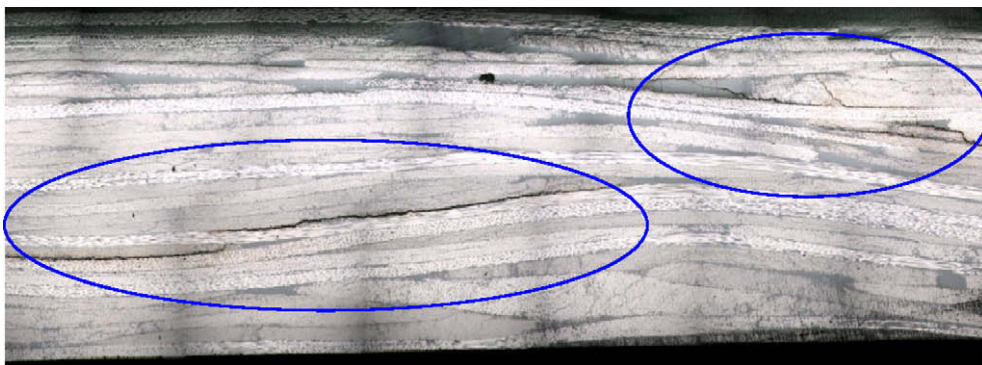
Fig. 18. Detail of section M2, far right.

Fig. 19. Detail of section M1, far right.

From these tests it can be concluded that 6 out of 7 notched specimens tested fail away from the open hole, and that no direct correlation can be extracted between this behavior and the presence of significant hot spots. Furthermore, during loading damage initiates away from the hole, and sometimes in apparently pristine regions. On the other hand, there appear to be no signs of damage initiation and propagation around the hole, typical of continuous fiber laminates.

5. Conclusions

A new material form is being considered for aircraft primary structural applications, and consists of discontinuous carbon fiber/epoxy random mat of chopped unidirectional prepreg tape. Commercial applications for this type of material form already exist, such as Hexcel HexMC®. Non-destructive inspection of these materials is difficult due to the heterogeneity of the chip distribu-
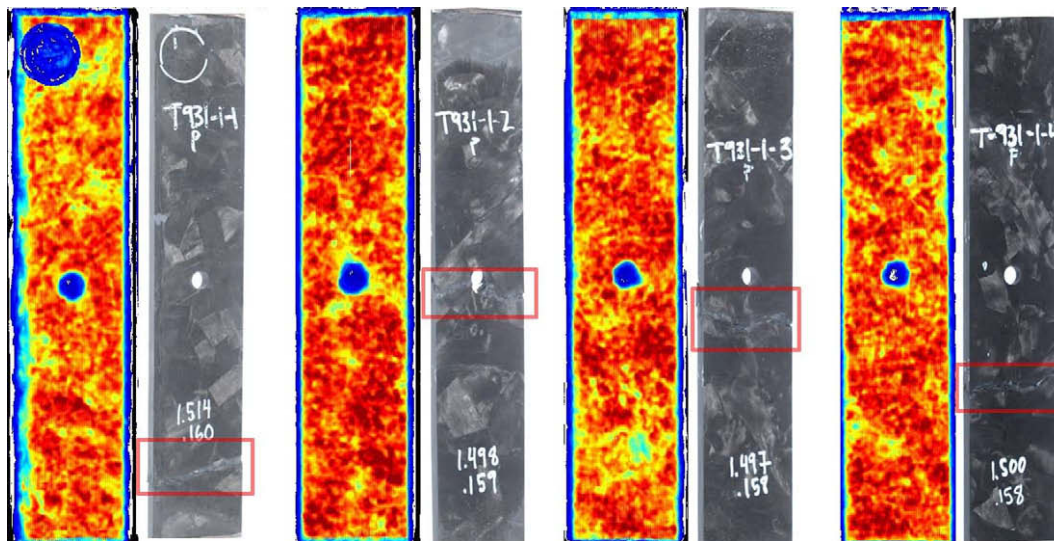
Fig. 20. Specimens #18–21, containing no evident hot spots, are loaded to failure in the presence of an open hole, and in 75% of cases lead to failure away from the hole.
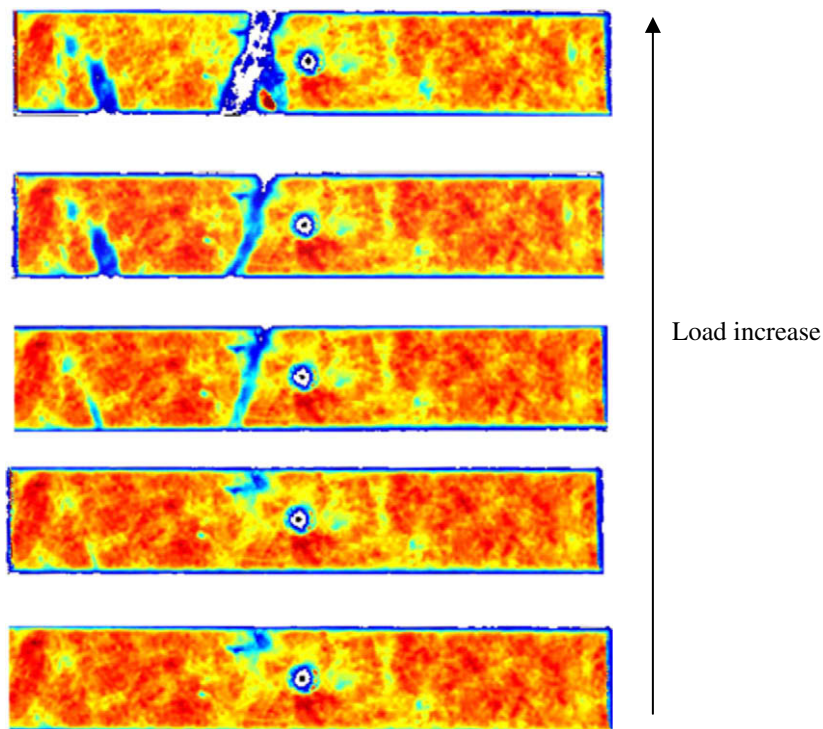
Fig. 21. Specimen #22 with an open hole undergoing progressive loading and ultrasonic imaging up to ultimate failure.

tion and orientation, which results in several regions of signal attenuation. A series of focused ultrasonic C-scan inspections, verified by the use of targeted microscopic analysis, have been used to characterize these regions of signal attenuations, referred to as "hot-spots". Previous studies by the authors have shown that these materials exhibit a particular notch-insensitive behavior, which is thought to be associated to the heterogeneous micro-structure of the material. It is found that these hot spots correspond to real defects, such as macro-voids (resulting from entrapped air in resin-starved regions), swirls (regions of fiber kinking resulting from high flow), or resin-rich pockets. There appears to be no way to

determine the type of the defect from non-destructive inspection alone. A series of tensile tests on pristine specimens, both unnotched and containing an open hole, are performed to measure the growth of these hot spots up to ultimate failure. It is found that failure is likely not to occur in proximity of these hot spots, independently from their size and location. For the notched specimens, in the vast majority of cases failure occurs away from the open hole and in most cases it precipitates in regions of apparently pristine micro-structure, that is away from evident hot spots. In conclusion, it appears that for this class of materials conventional ultrasonic inspection and defect classification for part acceptance may not
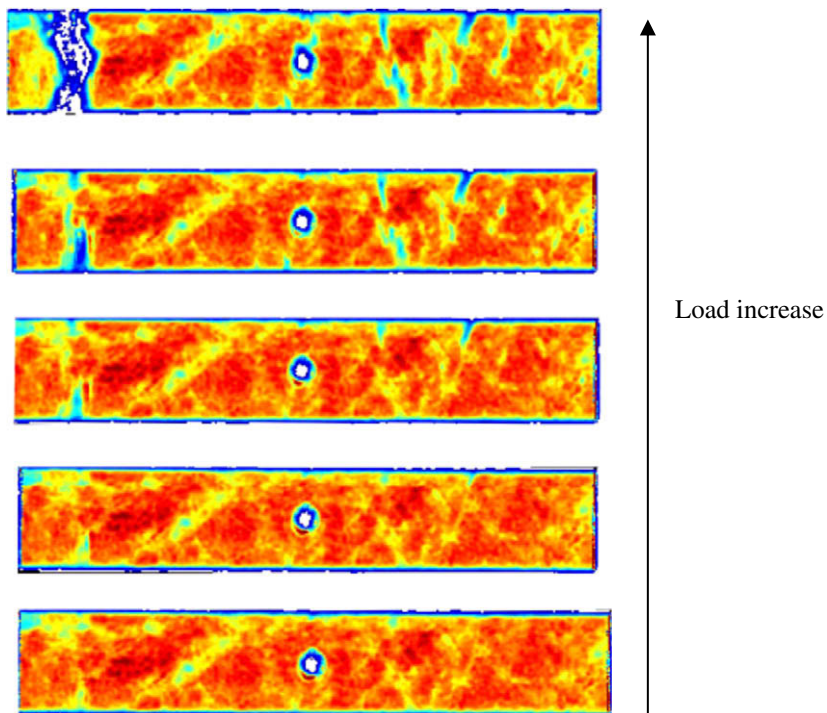
Fig. 22. Specimen #23 with an open hole undergoing progressive loading and ultrasonic imaging up to ultimate failure.
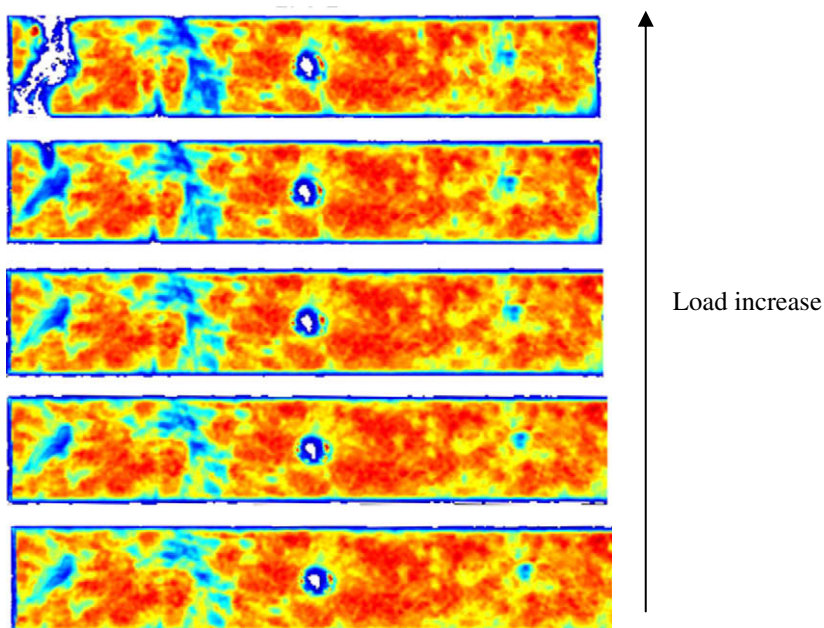
Fig. 23. Specimen #24 with an open hole undergoing progressive loading and ultrasonic imaging up to ultimate failure.

be adequate, and it could result in an unacceptable high rejection rate, without at the same time providing increased confidence in part integrity and performance.

References

[1] Halpin JC. Stiffness and expansion estimates for oriented short fiber composites. Polym Eng Sci 1969;3:732.
[2] Halpin JC, Pagano NJ. The laminate approx. for randomly oriented short fiber composites. Polym Eng Sci 1969;3:720.

[3] Kardos JL, Michno MJ, Duffy TA. Investigation of high performance short fiber reinforced plastics. Final Report, Naval Air Systems Command, No. N00019-73-C-0358; 1974.

[4] Boeing 787 features composite window frames, Reinforced plastics, Application News, 2007;51(3):4 [March].

[5] Porter J. Moving closer to the goal of cost effective complex geometry carbon composite parts, HPC4HPC special session. In: Proceedings of the 19th ASC technical conference, Atlanta, GA, September 2004.

[6] Feraboli P, Peitso E, Deleo F, Cleveland T, Stickler PB. Characterization of prepreg-based discontinuous carbon fiber/epoxy systems: Part I. J Reinf Plast Compos 2009;28(10):1191–214.

[7] Feraboli P, Peitso E, Cleveland T, Stickler PB, Halpin JC. Notched behavior of prepreg-based discontinuous carbon fiber/epoxy systems. Composites: Part A 2009;40(3):289–99.

[8] Feraboli P, Peitso E, Cleveland T, Stickler PB. Modulus measurement for prepreg-based discontinuous carbon fiber/epoxy systems. J Compos Mater 2009;43(19):947–1965.

[9] ASTM D3171-09. Standard test methods for constituent content of composite materials, vol. 15.03. West Conshohocken (PA): ASTM International; 2008.

[10] Boeing standard test method for unnotched tension, D6-83079-61. The Boeing Co.; 2008.